Available online at www.sciencedirect.com
ScienceDirect
Thin Solid Films 517 (2008) 1106–1110
www.elsevier.com/locate/tsf

Water adsorption on fullerene-like carbon nitride overcoats

E. Broitman [a,*], G.K. Gueorguiev [b], A. Furlan [b], N.T. Son [b], A.J. Gellman [a], S. Stafström [b], L. Hultman [b]

[a] Department of Chemical Engineering, Carnegie Mellon University, Pittsburgh, PA 15213, USA
[b] IFM, Linköping University, SE 581-83 Linköping, Sweden

Available online 24 July 2008

Abstract

Humidity influences the tribological performance of the head-disk interface in magnetic data storage devices. In this work we compare the uptake of water of amorphous carbon nitride (a-CN_x) films, widely used as protective overcoats in computer disk drive systems, with fullerene-like carbon nitride (FL-CN_x) and amorphous carbon (a-C) films. Films with thickness in the range 10–300 nm were deposited on quartz crystal substrates by reactive DC magnetron sputtering. A quartz crystal microbalance placed in a vacuum chamber was used to measure the water adsorption. Electron paramagnetic resonance (EPR) has been used to correlate water adsorption with film microstructure and surface defects (dangling bonds). Measurements indicate that the amount of adsorbed water is highest for the pure a-C films and that the FL-CN_x films adsorbed less than a-CN_x. EPR data correlate the lower water adsorption on FL-CN_x films with a possible lack of dangling bonds on the film surface.

To provide additional insight into the atomic structure of defects in the FL-CN_x, a-CN_x and a-C compounds, we performed first-principles calculations within the framework of Density Functional Theory. Emphasis was put on the energy cost for formation of vacancy defects and dangling bonds in relaxed systems. Cohesive energy comparison reveals that the energy cost formation for dangling bonds in different configurations is considerably higher in FL-CN_x than for the amorphous films. These simulations thus confirm the experimental results showing that dangling bonds are much less likely in FL-CN_x than in a-CN_x and a-C films.

Keywords: carbon nitride; CNx; dangling bonds; water adsorption; QCM; EPR; DFT

1. Introduction

The largest industrial application of sputtered carbon films containing hydrogen and/or nitrogen is in magnetic storage devices. In all cases, the deposited coatings are amorphous, containing hydrogen to saturate the dangling carbon bonds and to prevent oxidation, and containing nitrogen to improve the overcoat durability [1]. Recently, we have proposed the use of an alternative nanostructured carbon-based coating [2]. Resembling parts of a fullerene structure, it consists of sp^2-coordinated graphitic basal planes that are buckled due to the presence of pentagons and cross-linked at sp3-hybridized C sites, both of which are caused by structural incorporation of nitrogen [3]. This nanostructured coating, called fullerene-like carbon nitride (FL-CN_x), has many tribological advantages over amorphous a-CN_x in properties such as hardness, friction coefficient, wear resistance, and elastic recovery [4–7].

In this work we compare the uptake of water in amorphous carbon nitride (a-CN_x) films, widely used as protective overcoats in computer disk drive systems, with fullerene-like carbon nitride (FL-CN_x) and amorphous carbon (a-C) films. Electron paramagnetic resonance (EPR) is used to correlate water adsorption with film microstructure and surface defects (dangling bonds). To provide additional insight into the atomic structure of defects in the FL-CN_x, a-CN_x and a-C compounds, we perform first-principles calculations within the framework of Density Functional Theory (DFT).

2. Experimental details

Carbon films were deposited on quartz substrates by magnetron sputtering. A pure hot-pressed graphite target was reactively sputtered in an N_2/Ar (99.9999% purity) discharge at a variety of N_2 partial pressures by means of a DC unbalanced magnetron operated at a constant total pressure of 0.4 Pa and at a constant discharge current of 400 mA. CN_x coatings were deposited onto both sides of quartz crystals mounted in a biased

* Corresponding author.
E-mail address: broitman@andrew.cmu.edu (E. Broitman).

0040-6090/$ - see front matter © 2008 Elsevier B.V. All rights reserved.
doi:10.1016/j.tsf.2008.07.022

substrate holder that was rotated and resistively heated from the reverse side. More details on the deposition setup as well as a detailed process characterization can be found elsewhere [2,5]. EPR measurements were performed ex-situ at room temperature using a E580 Bruker X-band (~9.6 GHz) EPR spectrometer at 5 K with a field modulation of 0.25 G. For comparison, a commercial overcoat was also deposited on a quartz substrate; prior to the water adsorption study the sample was cleaned with a jet of dry air.

The apparatus designed and constructed for measurement of humidity adsorption on lubricated overcoats has been described previously [8]. It consists of a vacuum chamber that can be evacuated by a turbopump or a sorption pump and operates in the pressure range of 10^{-6}–10^{5} Pa. The turbopump is used initially to achieve a base pressure of 10^{-6} Pa, while the sorption pump is utilized during the experiments to avoid vibrations of the quartz crystal microbalance (QCM). A capacitance manometer was used to measure the partial pressure of water in the range 10^{1}–10^{5} Pa. The QCM housing is capable of holding 3 quartz crystals for simultaneously monitoring water adsorption on three surfaces. The temperature of the QCM is measured by a K-type thermocouple spot-welded to the quartz crystal housing. The QCM is controlled at 50 °C using flowing water. The mass of water adsorbed on the surface of the quartz crystal was calculated using the Sauerbrey equation $\Delta f = -C\,\Delta m$, where Δf and Δm are the change in frequency and the adsorbed mass of water, respectively [2].

3. Computational details

Finite model systems simulating a-C, a-CN_x, as well as systems in which N is incorporated in sp^2-hybridized graphene sheets (to represent FL-CN_x) were considered. The study involved both geometry optimizations and cohesive energy (E_{coh}) calculations performed within the DFT framework in its Generalized Gradient Approximation (GGA). Differences in cohesive energies $|\Delta E_{coh}|$ for the possible structures are determined by an optimization strategy presented elsewhere [9,10], making use of the GAUSSIAN 03 program [11]. For the DFT-GGA, the Perdew–Wang exchange-correlation functional (PW91) [12] and the B3LYP hybrid functional [13] were used. Both are known to provide an accurate description of the structural and electronic properties of FL thin films [9,10] and similar covalent systems [14–16]. For both carbon and nitrogen, double-ζ basis sets augmented with polarization functions were used. The results reported in this work correspond to PW91 exchange-correlation functional while B3LYP simulations were reserved for test purposes.

4. Results and discussion

4.1. Film composition and structure

CN_x coatings were grown at different bias voltages, N_2 pressures and substrate temperatures (T_s) in order to synthesize FL-CN_x and a-CN_x coatings as well as nitrogen-free graphite (a-C_{sp2}) and DLC (a-C) type coatings (Table 1).

Pure carbon coatings are known to form an amorphous and low density structure at higher temperatures and low ion bombardment, due to the formation of exclusively sp^2-hybridized carbon into aromatic structures [5,17]. This is the case for the sample grown in a pure Ar discharge at T_s=450 °C and V_{Bias}=−25 V (sample a-C_{sp2}, Table 1). If the growth temperature is lowered, as for the sample grown at 150 °C and −25 V (sample a-C), sp-hybridized carbon generated by ion bombardment is incorporated and the aromatic sp^2-hybridized structures network is disrupted; hence, denser amorphous coatings can be formed [5,17].

Table 1
Deposition parameters for the analyzed films along with their composition, densities and respective growth rates

Name	N_2 fraction in plasma	$T_{substrate}$ (°C)	V_{Bias} (V)	$C_{nitrogen}$ (at.%) (a)	Density (g cm^{-3}) (a)	Growth rate (10^{-1} nms^{-1}) (a)
a-C	0	150	25	–	2.1	0.42
a-C_{sp2}	0	450	25	–	0.6	1.52
FL-CN_x	0.16	450	25	17	2.2	0.35
a-CN_x	1	150	25	25±5%	2.3±0.6%	0.95
a-CH_y	Commercial overcoat provided by Seagate Inc. containing ~20% of H					

Values in (a) are from ref. [5].

When the films are grown at T_s=450 °C with 16% nitrogen present in the sputtering gas (sample FL-CN_x), plan-view transmission electron microscopy indicates a FL-structure in the form of curved basal planes resembling the arrangement of a leek or onion, but with buckling and interlinking of atomic planes [17]. At lower substrate temperature (150 °C), the desorption of volatile nitrogen-containing species from the growth surface during deposition (chemical sputtering) is suppressed, the FL-sheets are no longer observable and the material is considered amorphous [5]. This is the case for the coating grown in a pure N_2 discharge at T_s=150 °C (sample a-CN_x).

4.2. Adsorption of H_2O on CN_x overcoats

Fig. 1 shows the adsorption of water versus the water vapor pressure for films deposited under different conditions (see Table 1). For comparison, the adsorption of water on a commercial overcoat (a-CH_y) is also indicated. All carbon-based films show a characteristic dependence of water coverage on the H_2O vapor pressure. There are, however, differences in the amounts of the adsorbed water thus defining three different groups of films:

i) FL-CN_x and a-C_{sp2} show the lower adsorption rate. Taking into consideration one monolayer coverage is roughly 30 ng/cm^2 [2] and that at room temperature 1.33×10^3 Pa of H2O vapor pressure is equivalent to 50% RH, these films adsorb less than 2 ML at that pressure;
ii) a-CN_x and the commercial a-CH_y, have adsorbed roughly 2–3 times more water than the first group.
iii) Finally, a-C adsorbs more than 14 times the amount adsorbed by FL-CN_x.

There are very few comparative studies on the adsorption of water on carbon films with different microstructure and/or composition [2]. Smallen [18] investigated the water adsorption

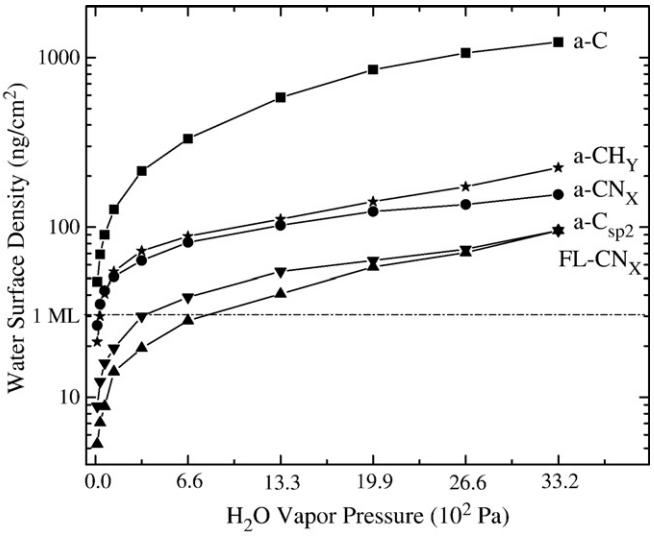

Fig. 1. The mass of water adsorbed on the surface of quartz crystal with carbon overcoats at 50 °C versus pressure. The dotted line indicates the value of 1 ML of H_2O on the surface.

of CH_y films deposited by sputtering in different Ar-C_2H_2 gas mixtures (0 to 30% of C_2H_2). Their ellipsometric measurements of the thickness of adsorbed water have shown that the adsorption increased with the relative humidity and concentration of hydrogen in the film. Lee [19] studied indirectly the adsorption of water on a-CN_x films. He measured the electrical properties of the coatings as a function of ambient humidity, and proposed the a-CN_x film as a novel humidity sensor. In a previous work, we have compared the electrical properties of a-C, a-CN_x and FL-CN_x films [20]. We reported that after exposure to atmosphere, FL-CN_x films were unaffected by humidity, while a-C films were very sensitive to H_2O vapor exposure. In a recent publication, we have also reported the adsorption of water on lubricated carbon overcoats [2].

It has been shown that the adsorption of water on carbon films is proportional to the hydrogen content of the overcoats [18]: the incorporation of hydrogen into the carbon structure makes the film more polar. As all our films (except a-C) have an amount of hydrogen below 0.1% [20], they should adsorb less water than a-CH_y. However, Fig. 1 indicates that this is not the case. The differences in adsorption on our films must be understood in the context of their microstructural and morphological differences.

The surface of the sputtered carbon-based films is heterogeneous and is composed of different hybridized carbon atoms (sp, sp^2, and sp^3) and dangling bonds. As soon as the surface is exposed to air, its dangling bonds react with oxygen and form oxygen containing polar groups such as C–O–C, C–OH, C–H, and C=O [21,22]. Because of the hydrogen bonding tendency of water, the adsorption of water is sensitive to the polarity of the adsorbent surface [18] and is enhanced by the presence of oxidized carbon. We should expect that, because of the fullerene structure, FL-CN_x films have the lowest number of dangling bonds and, in consequence, low water adsorption. ESR measurements confirm our assumption: Fig. 2 shows that, in contrast to a-CN_x films, the FL-CN_x coating has no ESR signal, i.e., very low number of dangling bonds.

The surface roughness could also play an important role on the water adsorption, as pointed out by Smallen [18]. In [20] we found that the a-C sample has an rms roughness of 15 nm, the a-CN_x has 2.5 nm, while FL-CN_x has the lowest roughness (rms=0.4 nm). The surface roughness seems to correlate well with the water adsorption shown in Fig. 1. However, surface roughness only plays a role in the adsorption of water at high levels of RH, where capillary condensation can occur in the valleys giving thicker water films [2].

4.3. Theoretical modeling

4.3.1. Energy cost for defects as a measure for occurrence of dangling bonds in FL-CN_x

Different model systems containing pentagons defects have been shown to correctly describe FL-CN_x [9,10]. Both curved two-dimensional graphene layers [10] and cross-linked structures [9] have been previously addressed from point of view of synthetic growth of FL-CN_x. In the present work, we consider typical FL-CN_x model systems, focusing specifically on the cohesive energy cost for formation of defects associated with dangling bonds.

Fig. 3 displays three FL-CN_x model systems. In the first row, the curved model system 1 contains a pentagon. In the second row, model system 2, contains a double pentagon defect, while in the third row the model system 3 contains a cross-linkage. In the first column — the structural variants 1a, 2a, and 3a do not contain dangling bonds, in the second column — variants 1b, 2b and 3b contain a dangling bond due to a pyridine-like defect, and finally, in the third column — variants 1c, 2c, 3c simulate a peripheral dangling bond.

The cohesive energy E_{coh} of a model system is defined as the energy required for breaking the system into isolated atomic species, i.e.,

$$E_{coh} = E_{total} - \sum_i E_{i,total}^{isolated},$$

i stays for different constituent atoms. In Table 2 the PW91 E_{coh} for the structures displayed in Figs. 3 and 4 are listed. ΔE_{coh}

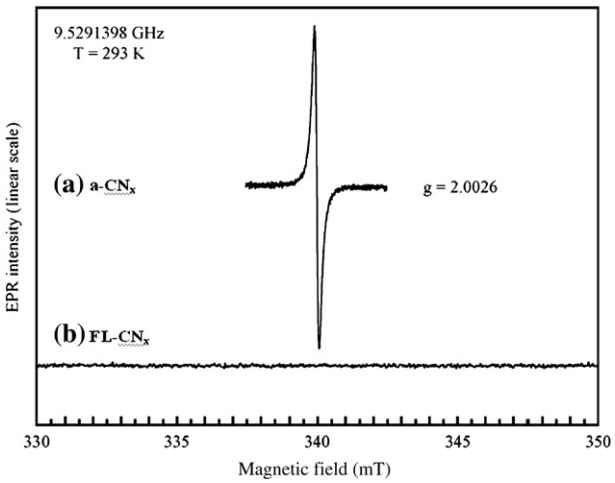

Fig. 2. Electron spin resonance from (a) amorphous CN_x film and (b) FL-CN_x film.

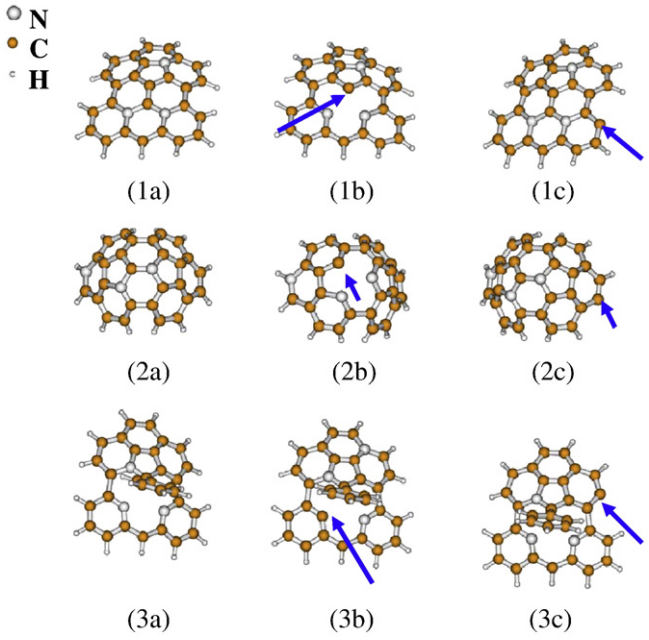

Fig. 3. The considered FL-CN_x model systems: In the first row the model system 1 is containing a pentagon: (1a) configuration without dangling bonds; (1b) system with a dangling bond due to a pyridine-like defect; (1c) model structure with a dangling bond at its edge; In the second row the system 2 corresponds to strongly curved graphene layer containing a double pentagon defect and41: (2a) without dangling bonds; (2b) with a dangling bond due to a pyridine-like defect; (2c) with a dangling bond at its edge; In the third row the system 3 incorporates a cross-linkage: (3a) without dangling bonds; (3b) with a dangling bond due to a pyridine-like defect; (3c) with a dangling bond at its edge; In all figures the arrow indicates the location of the dangling bond.

stays for the energy cost for dangling bonds formation with reference to the analogous structures but without dangling bonds (Fig. 3.1a, 2a, and 3a).

The results listed in Table 2 show that the energy cost for a dangling bond associated with a pyridine-like defects is by 0.05–0.26 eV lower than that for a dangling bond at a peripheral site. However, for both types of dangling bonds the energy cost is the highest for a slightly curved graphene sheet (Fig. 3, first row) , lower for a considerably more curved graphene plane (Fig. 3, second row), and lowest for a cross-linked structure (Fig. 3, third row). While the first row system in Fig. 3 can be seen as simulating the surface of solid FL-CN_x, the systems in the other two rows display important structural features of FL-CN_x in depth of the film — stronger curved sheets (second row), and cross-linkages (third row). Thus, the present E_{coh} data indicates that the formation of dangling bonds at the FL-CN_x surface is considerably less favorable, by approximately 0.2–0.6 eV, than in depth of the same material. Such energy differences ΔE_{coh} are several times larger than the thermal energy at growth environment temperatures ~0.065 eV. Consequently, ΔE_{coh} appears as an appropriate criterion for likeliness of structural features in carbon-based compounds.

In addition, the E_{coh} data suggests that the occurrence of dangling bonds is less likely in well-structured FL-CN_x with lower nitrogen content (5–15 at.%) for which slightly curved graphene sheets and lower density of cross-linkages are expected [9].

Table 2
PW91 cohesive energies E_{coh} corresponding to the model systems displayed in Figs. 3 and 4

		a (no dangling bonds)	*b* (pyridine-like)	*c* (peripheral)
FL-CN_x	E_{coh} (eV)	10.65	9.31	9.26
Model 1	ΔE_{coh} (eV)	0	1.34	1.39
FL-CN_x	E_{coh} (eV)	10.37	9.21	9.05
Model 2	ΔE_{coh} (eV)	0	1.16	1.32
FL-CN_x	E_{coh} (eV)	9.89	9.18	8.92
Model 3	ΔE_{coh} (eV)	0	0.71	0.97
a-CN_x	E_{coh} (eV)	11.78	11.19	–
	ΔE_{coh} (eV)	0	0.59	–
a-C	E_{coh} (eV)	12.45	11.98	–
	ΔE_{coh} (eV)	0	0.47	–

$\Delta E_{coh} = E_{coh}$(model system with a dangling bond) $- E_{coh}$ (analogous model system but without dangling bonds).

In FL-CN_x the energy cost for non-pyridine-like dangling bonds is always higher. Most non-pyridine-like defects, except the ones forcedly created at the edge of the model systems (Fig. 3.1.c, 2.c and 3.c) do not prevail along the optimization procedure. Instead, during the stepwise relaxation, the competition between different defects leads to atomic rearrangement and to an efficient saturation of the non-pyridine-like dangling bonds by formation of pentagon defects, Stone–Wales defects and cross-linkages as discussed in details in Ref. [9].

4.3.2. Energy cost for dangling bonds in a-CN_x and a-C

The lower energy cost for dangling bonds in CN_x structures containing cross-linkages suggests that higher occurrence of dangling bonds can be expected when CN_x compounds get gradually less ordered (or more amorphous), e.g., by formation of increasingly curved and/or interlocked graphene sheets. Such material can be seen as a structural transition between FL-CN_x and a-CN_x.

To compare the cost for dangling bonds in a-CN_x and a-C to the data reported above for FL-CN_x, we optimize model systems representing amorphous compounds which contain a mixture of sp^2/sp^3-coordinated networks. Fig. 4a and b shows a-CN_x

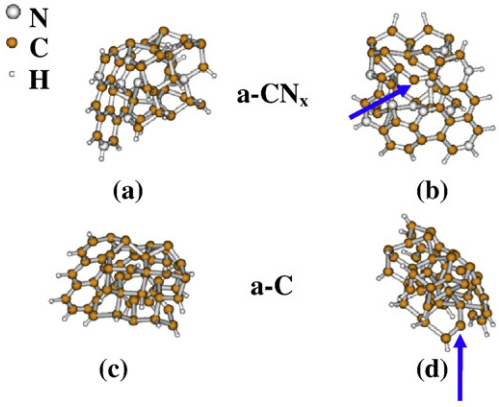

Fig. 4. a-CN_x (top row) and a-C (bottom row) model systems: (a) and (c) without a dangling bond; (b) and (d) with a dangling bond (the arrows point to the location of the dangling bond).

systems without and with a pyridine-like dangling bond, respectively. The reason to emphasize again the pyridine-like vacancy resulting in a dangling bond is that, similarly to FL-CN_x, in a-CN_x it has the lowest energy cost. In a-CN_x, the pyridine-like dangling bond is by E_{coh}~0.1–0.2 eV more favorable than dangling bonds simulated by unpaired electron at given C site at the edge of the model system. Provided that the energy difference between pyridine-like and non-pyridine-like defects is considerably lower than in FL-CN_x, it is likely that in a-CN_x pyridine-like dangling bonds coexist with other types of dangling bonds.

As seen from Table 2, in a-CN_x (Fig. 4a and b) the energy cost for pyridine-like vacancies is 0.59 eV (to be compared to 0.71–1.34 eV for FL-CN_x) i.e., higher density of dangling bonds is expected in a-CN_x solid material.

Fig. 4c and d shows configurations analogous to those in Fig. 4a and b but corresponding to pure amorphous carbon. Obviously, in the case of a-C no pyridine-like vacancies are possible, the dangling bonds naturally resulting from the relaxation of the amorphous C network. A typical model system representing a-C consists of randomly interconnected pieces of graphene sheets which after relaxation evolve to a mixed mostly sp^2/sp^3-coordinated C network. In the absence of nitrogen, neither pentagon-containing curved graphene planes nor such variety of geometrically well-defined defects, like in FL-CN_x, are possible. Importantly, in a-C the energy cost for a dangling bond is by ~0.1 eV lower than in a-CN_x and by ~0.3–0.9 eV (depending on the type of defect) lower than in FL-CN_x (see Table 2). Thus in a-C, the likeliness of dangling bonds is considerably higher than in FL-CN_x, and still somehow higher than in a-CN_x.

5. Conclusions

QCM measurements have probed the effect of microstructure and composition of carbon on overcoat surfaces on the adsorption of water. The microstructure and chemistry influences the adsorption level; amorphous coatings absorb significantly more water than the fullerene-like carbon nitride films. EPR data correlates the lower water adsorption on FL-CN_x films with a possible lack of dangling bonds on the film surface.

First-principles calculations reveal that the energy cost for different types of dangling bonds in different configurations is considerably higher in FL-CN_x than for amorphous films, being the lowest to pure a-C. Thus, our simulations confirm the experimental results showing that dangling bonds are much less likely in FL-CN_x than in a-CN_x and a-C films.

The water adsorption of fullerene-like carbon nitride films is lower than on the commercial a-CH_y overcoats. Taking into consideration their superior tribological properties, FL-CN_x overcoats have a potential application in the hard disk industry.

Acknowledgments

The authors acknowledge V.V. Pushkarev from Carnegie Mellon University for some of the measurements shown in Fig. 2. E.D.B. and A.J.G. acknowledge the Data Storage Systems Center (DSSC) at Carnegie Mellon University. G.K.G. gratefully acknowledges The Swedish Research Council (VR) and the European Commission under the project FOREMOST. AF and LH acknowledge The Swedish Foundation for Strategic Research (SSF). We thank Seagate Inc. for supplying the a-CH_Y samples.

References

[1] E.V. Anoikin, M.M. Yang, J.L. Chao, J.R. Elings, D.W. Brown, J. Vac. Sci. Technol., A, Vac. Surf. Films 16 (3) (1998) 1741.
[2] E. Broitman, V.V. Pushkarev, A.J. Gellman, J. Neidhardt, A. Furlan, L. Hultman, Thin Solid Films 515 (3) (2006) 979.
[3] L. Hultman, J. Neidhardt, N. Hellgren, H. Sjostrom, J.E. Sundgren, MRS Bull. 28 (3) (2003) 194.
[4] E. Broitman, N. Hellgren, O. Wanstrand, M.P. Johansson, T. Berlind, H. Sjostrom, J.E. Sundgren, M. Larsson, L. Hultman, Wear 248 (1–2) (2001) 55.
[5] J. Neidhardt, L. Hultman, E. Broitman, T.W. Scharf, I.L. Singer, Diamond. Relat. Mater. 13 (10) (2004) 1882.
[6] E. Broitman, W. Macdonald, N. Hellgren, G. Radnoczi, Z. Czigany, A. Wennerberg, M. Jacobsson, L. Hultman, Diamond. Relat. Mater. 9 (12) (2000) 1984.
[7] E. Broitman, W.T. Zheng, H. Sjostrom, I. Ivanov, J.E. Greene, J.E. Sundgren, Appl. Phys. Lett. 72 (20) (1998) 2532.
[8] N. Shukla, E. Svedberg, R.J.M. van der Veerdonk, X. Ma, J. Gui, A.J. Gellman, Tribol. Lett. 15 (1) (2003) 9.
[9] G.K. Gueorguiev, J. Neidhardt, S. Stafstrom, L. Hultman, Chem. Phys. Lett. 410 (4–6) (2005) 228.
[10] G.K. Gueorguiev, J. Neidhardt, S. Stafstrom, L. Hultman, Chem. Phys. Lett. 401 (1–3) (2005) 288.
[11] M.J. Frisch, GAUSSIAN 03, Gaussian, Inc., Wallingford, CT, 2003.
[12] J.P. Perdew, J.A. Chevary, S.H. Vosko, K.A. Jackson, M.R. Pederson, D.J. Singh, C. Fiolhais, Phys. Rev. B 46 (11) (1992) 6671.
[13] A.D. Becke, J. Chem. Phys. 98 (7) (1993) 5648.
[14] S. Stafstrom, L. Hultman, N. Hellgren, Chem. Phys. Lett. 340 (3–4) (2001) 227.
[15] R.H. Xie, G.W. Bryant, L. Jensen, J.J. Zhao, V.H. Smith, J. Chem. Phys. 118 (19) (2003) 8621.
[16] R.H. Xie, G.W. Bryant, V.H. Smith, Chem. Phys. Lett. 368 (3–4) (2003) 486.
[17] E. Broitman, N. Hellgren, K. Jarrendahl, M.P. Johansson, S. Olafsson, G. Radnoczi, J.E. Sundgren, L. Hultman, J. Appl. Phys. 89 (2) (2001) 1184.
[18] M. Smallen, J.K. Lee, A. Chao, J. Enguero, IEEE Trans. Magn. (1994) 4137.
[19] L.G. Lee, S.L. Lee, Sens. Actuators B 108 (2005) 450.
[20] E. Broitman, N. Hellgren, J. Neidhardt, I. Brunell, L. Hultman, J. Electron. Mater. 31 (9) (2002) L11.
[21] N. Shukla, A.J. Gellman, J. Gui, Langmuir 16 (16) (2000) 6562.
[22] R.H. Wang, R.L. White, S.W. Meeks, B.G. Min, A. Kellock, A. Homola, D. Yoon, IEEE Trans. Magn. 32 (5) (1996) 3777.